Hindawi Publishing Corporation
Mathematical Problems in Engineering
Volume 2015, Article ID 682321, 14 pages
http://dx.doi.org/10.1155/2015/682321

*Research Article*

# Modeling and Coordinated Control Strategy of Large Scale Grid-Connected Wind/Photovoltaic/Energy Storage Hybrid Energy Conversion System

**Lingguo Kong,[1] Guowei Cai,[1] Sidney Xue,[2] and Shaohua Li[2]**

[1]*School of Electrical Engineering, Northeast Dianli University, Jilin 132012, China*
[2]*China Datang Corporation Science and Technology Research Institute, Beijing 102206, China*

Correspondence should be addressed to Lingguo Kong; klgwin@hotmail.com

Received 24 May 2014; Revised 17 July 2014; Accepted 17 July 2014

Academic Editor: Hui Zhang



An AC-linked large scale wind/photovoltaic (PV)/energy storage (ES) hybrid energy conversion system for grid-connected application was proposed in this paper. Wind energy conversion system (WECS) and PV generation system are the primary power sources of the hybrid system. The ES system, including battery and fuel cell (FC), is used as a backup and a power regulation unit to ensure continuous power supply and to take care of the intermittent nature of wind and photovoltaic resources. Static synchronous compensator (STATCOM) is employed to support the AC-linked bus voltage and improve low voltage ride through (LVRT) capability of the proposed system. An overall power coordinated control strategy is designed to manage real-power and reactive-power flows among the different energy sources, the storage unit, and the STATCOM system in the hybrid system. A simulation case study carried out on Western System Coordinating Council (WSCC) 3-machine 9-bus test system for the large scale hybrid energy conversion system has been developed using the DIgSILENT/Power Factory software platform. The hybrid system performance under different scenarios has been verified by simulation studies using practical load demand profiles and real weather data.

## 1. Introduction

Recently, pollutants in the air are progressing in correlation with the increasing consumption of energy. The ever-increasing demand for conventional energy sources like coal, natural gas, and crude oil is driving society towards the research and development of alternative environmentally friendly energy sources. Thus the renewable energy sources (RES) should play a significant role [1, 2]. Among these RES available the wind energy conversion system (WECS) and solar photovoltaic (PV) generation system are the most widely used ones, since their technological progress has made them promising, mature, cost-effective, and reliable [3–5]. Wind energy is the fastest growing energy technology in terms of percentage of yearly growth of installed capacity per technology source [6–8]. The applications PV systems have become more widespread in both developed and developing countries. In order to efficiently and economically utilize large scale renewable energy resources of wind and PV applications, some form of backup and smoothing power fluctuation systems are almost universally required [9, 10]. Energy storage (ES) system is very important for wind-solar power generation systems [11–13]. The details of the system configuration and the characteristics of the major system components are discussed in this paper. An overall power coordinated control strategy is designed for the system to coordinate the power flows among the diverse energy sources. Simulation studies have been carried out to verify the system performance under different scenarios using practical load profiles and real weather data.

In this paper, a hybrid energy conversion system model consisting of wind, PV, and ES unit is proposed. Wind and PV are the primary power sources of the system to take full advantage of renewable energy. The ES combination is used as a backup and power control system, and static synchronous compensator (STATCOM) unit is also used in the hybrid

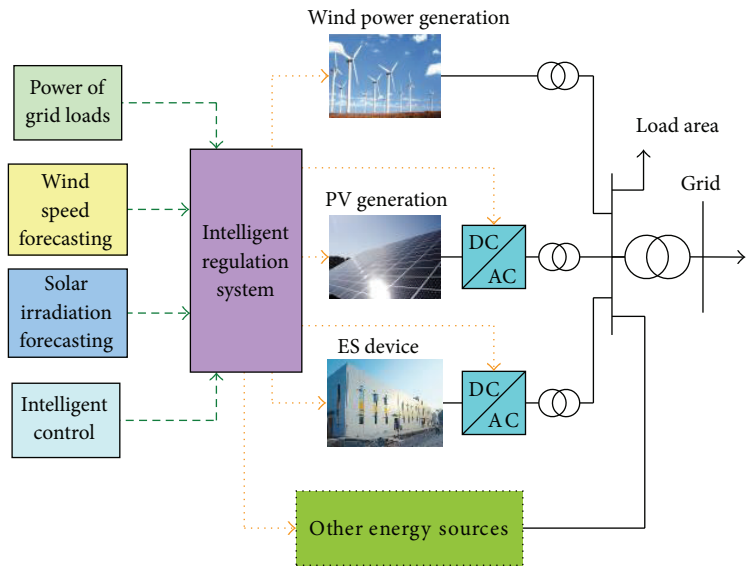


Figure 1: Configuration of the proposed grid-connected wind/PV/ES hybrid energy.

system for reactive backup and enhances the low voltage ride through (LVRT) capability.

## 2. Configuration of Grid-Connected Hybrid System

Figure 1 shows the proposed configuration applied to a combined large scale hybrid energy system integrating three main subsystems of wind, PV, and ES with an intelligent control unit. The wind and PV systems are used as primary energy source and the ES device as a backup energy source. All three energy systems are connected in parallel to a common AC bus line through three individual nonisolated power control units [14, 15]. The outputs from the three different power sources are integrated on the AC bus line to provide the desired power to the power network and grid-connected load even if only one source is available, and the others are diminished. Doubly fed induction generators (DFIGs) are adopted for wind power generation system. The DC-AC converters are employed for synchronous incorporation into the network of PV system. The additional DC-AC converters are used to control the ES system for load or grid power fluctuation. STATCOM system is used as an auxiliary unit to regulate reactive power and enhance the LVRT capability of the hybrid system. Different energy sources are connected to the AC bus through the appropriate power electronic interfacing circuits. The system can be easily expended; that is, other energy sources can be integrated into the system when they are available, as shown in Figure 1. The main system component models and characteristics are discussed in the following section.

## 3. System Description and Modeling

This section provides basic concepts of the proposed hybrid system, sums up the performance equations which were implemented in the simulated model, and discusses the control strategy of the WECS, PV generation system, and ES system included battery and FC stack, respectively.

*3.1. Wind Energy Conversion System.* The fundamental equation governing the mechanical power capture of the wind turbine rotor blades, which drives the DFIG considered in this paper, is given by

$$P_{\text{wind}} = \frac{1}{2}\rho A v^3 C_p(\lambda, \theta), \quad (1)$$

where $\rho$ is the air density (kg/m$^3$), $A$ is the area swept by the rotor blades (m$^2$), and $v$ is the wind velocity (m/s). $C_p$ is called the power coefficient or the rotor efficiency and is a function of tip speed ratio (TSR or $\lambda$) and pitch angle ($\theta$) [14–17].

A doubly fed induction generator (DFIG) model [17–20] was developed and used as a part of the wind energy change system (WECS). The details of the DFIG dynamic model have been used for all components of the system as shown in Figure 2. The component and controller parameters of the DFIG are given in Table 1.

Figure 3 shows the output power of the DFIG versus wind speed. It can be observed that the output power is kept constant when wind speed is higher than the rated wind velocity even though the wind turbine has the potential to produce more power. When wind speed is higher than the cutout speed (21.5 m/s), the system is taken out of operation for protection of its components.

WECS is composed of 100-DFIG model (see Figure 2) and booster transformer, and its rating capacity is 200 MW, which is due to the assumption made that the WECS components are ideal and the losses are negligible.

*3.2. Photovoltaic Generation System.* PV effect is a basic physical process through which solar energy is converted directly into electrical energy. The physics of a PV cell is similar to the classical p-n junction diode [21–23]. To increase

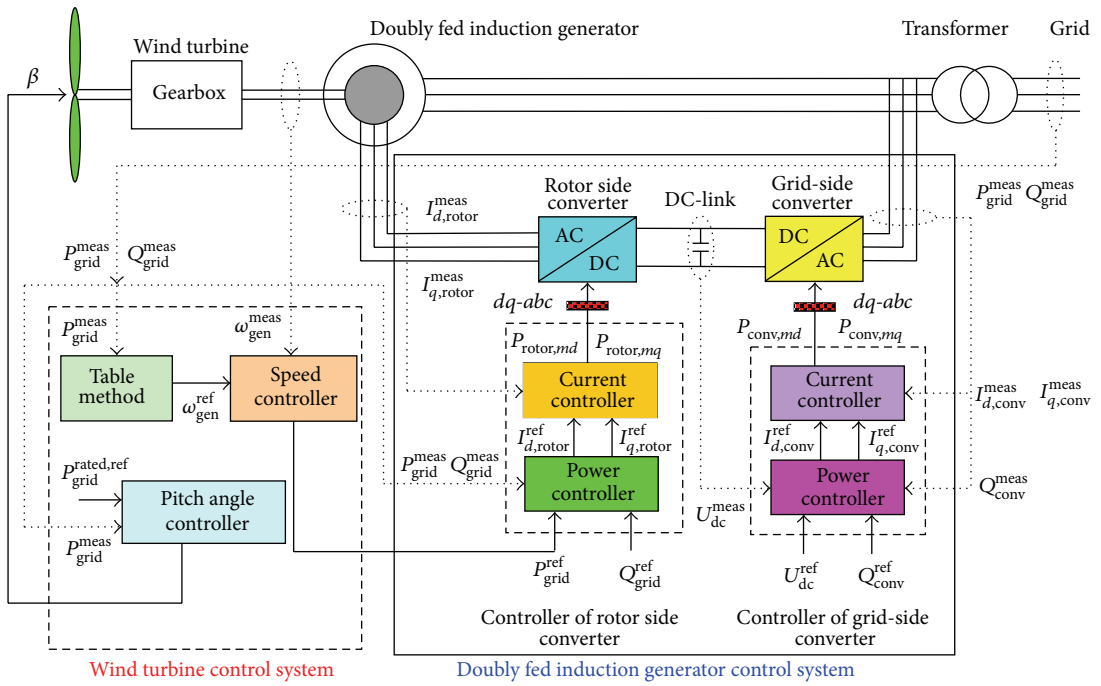


Figure 2: Block diagram of the overall control scheme for variable speed wind turbines with DFIG.

Table 1: Wind energy conversion system component parameters.

| Parameter | Value |
|---|---|
| Wind turbine | |
| Rated power | 2 MW |
| Cut in speed (cut out speed) | 6.2 m/s (21.5 m/s) |
| Rated speed | 11 m/s |
| Doubly fed induction generator (DFIG) | |
| Rated power | 2 MW |
| Rated voltage | 0.69 kV |
| Stator resistance (resistance) | 0.04 pu (0.1 pu) |
| Rotor resistance (reactance) | 0.01 pu (0.1 pu) |
| Inertia | 75 kg·m$^2$ |
| Proportional and integral gain of controller | |
| $K_p$ of speed controller | 1 |
| $T_i$ of speed controller | 0.1 |
| $K_p$ of pitch angle controller | 150 |
| $T_i$ of pitch angle controller | 25 |
| $K_p$ of power controller | 4 |
| $T_i$ of power controller | 0.1 |
| $K_p$ of current controller | 0.0496 |
| $T_i$ of current controller | 0.0128 |

the power, a multitude of PV cells is electrically connected to form larger units, called PV modules or array.

The relationship between the output voltage $V$ and the load current $I$ of a PV array or a module can be expressed as [24, 25]

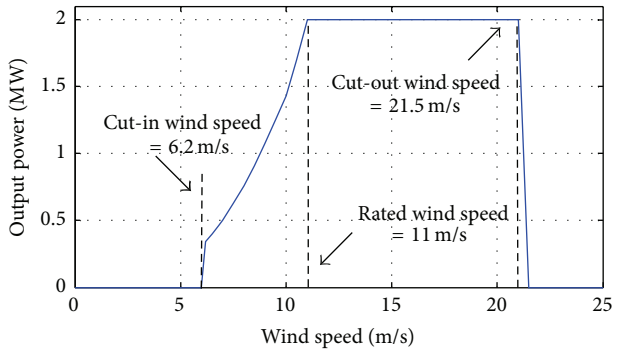


Figure 3: Wind turbine output power characteristic.

$$I_{\mathrm{PV}} = N_{\mathrm{PV}\text{-}p} I_{\mathrm{sc}} \cdot \left\{1 - C_1 \left[\exp\left(\frac{V_{\mathrm{PV}} - dV}{C_2 N_{\mathrm{PV}\text{-}s} V_{\mathrm{oc}}}\right) - 1\right]\right\} + dI, \tag{2}$$

where

$$C_1 = \left(1 - \frac{I_m}{I_{\mathrm{sc}}}\right) \cdot \exp\left(\frac{-V_m}{C_2 V_{\mathrm{oc}}}\right),$$

$$C_2 = \frac{V_m/V_{\mathrm{oc}} - 1}{\ln\left(1 - I_m/I_{\mathrm{sc}}\right)}, \tag{3}$$

$$dI = -\alpha \cdot \frac{G}{G_{\mathrm{ref}}} \cdot (T_c - T_{\mathrm{ref}}) + \left(\frac{G}{G_{\mathrm{ref}}} - 1\right) \cdot N_{\mathrm{PV}\text{-}p} I_{\mathrm{sc}},$$

$$dV = \beta \cdot dT - R_s \cdot dI,$$

where $I_{\mathrm{PV}}$ is the load current of PV array (A), $V_{\mathrm{PV}}$ is the output voltage of PV array (V), $T_{\mathrm{ref}}$ and $G_{\mathrm{ref}}$ are the reference cell

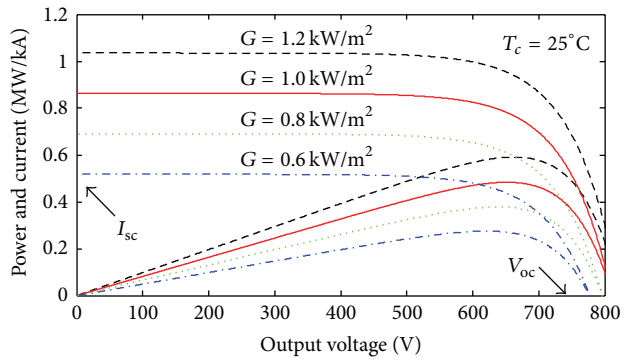


FIGURE 4: $I$-$V$ and $P$-$V$ characteristic curves of a PV array model at four irradiance levels.

temperature (25°C) and given solar irradiance (1000 W/m$^2$), $T_c$ is the actual operating temperature of the PV cell (°C), $G$ is the solar irradiance (W/m$^2$), and $R_s$ is the series resistance of PV cell (Ω). The power injected by PV array into the hybrid system could be written as

$$P_{\mathrm{PV}} = I_{\mathrm{PV}} V_{\mathrm{PV}} \left(1 - K_{\text{PV-loss}}\right). \tag{4}$$

The $I$-$V$ and $P$-$V$ characteristic curves of the PV model used in this study under different irradiances (at 25°C) are given in Figure 4. It is noted from the figure that the higher the irradiance, the larger the short circuit current ($I_{\mathrm{sc}}$) and the open circuit voltage ($V_{\mathrm{oc}}$) [25].

The details of the PV dynamic model have been used for all components of the unit shown in Figure 5. By using the perturbation and observation (P&O) method based on power change rate shown in Figure 6 and comparison repeatedly, the output power of the solar modules can then reach its maximum working point gradually [26]. The parameters and data of the PV generation unit are summarized in Table 2. The rating capacity of PV generation system that includes 200 PV units (see Figure 5) is 100 MW.

*3.3. Energy Storage System.* Battery stack [27, 28] and fuel cell (FC) unit [29–33] have been modeled for this study as two types of energy storage device. The dynamic model of a lead-acid battery is described for applications in power supply system. The inputs of the model are the electric power, ambient temperature, and mean value of the discharge current. Therefore, the battery stack or module can be expressed as

$$V_B = N_{B\text{-}s} E_0 - \frac{K\mathrm{SOC}}{\mathrm{SOC} - N_{B\text{-}s} Q_n \int_0^t i_B(\tau)\, d\tau} + A \exp\left(-B \int_0^t i_B(\tau)\, d\tau + C_P\right) - \frac{R i_B}{N_{B\text{-}s}}, \tag{5}$$

TABLE 2: PV generation system component parameters.

| Parameter | Value |
|---|---|
| PV array | |
| Open circuit voltage, $V_{\mathrm{oc}}$ | 45 V |
| Short circuit current, $I_{\mathrm{sc}}$ | 5.5 A |
| Maximum power voltage, $V_m$ | 36 V |
| Maximum power current, $I_m$ | 5 A |
| Temperature coefficients of current, $\alpha$ | 0.0025 |
| Temperature coefficients of voltage, $\beta$ | 0.0005 |
| Series resistance of cell, $R_s$ | 0.02 Ω |
| Dynamic link loss factor, $K_{\text{PV-loss}}$ | 0.05 |
| Number of series modules, $N_{\text{PV-}s}$ | 18 |
| Number of parallel modules, $N_{\text{PV-}p}$ | 155 |
| MPPT controller | |
| Low limit of power change rate (up limit), $\varepsilon_1$ ($\varepsilon_2$) | 60 W (4600 W) |
| Correction factor of power change rate, $\gamma$ | 0.00001 |
| Factor of voltage perturbation, $\xi$ | 1 |
| Proportional and integral gain of controller | |
| $K_p$ of power controller | 0.05 |
| $T_i$ of power controller | 0.0005 |
| $K_p$ of current controller | 1 |
| $T_i$ of current controller | 0.01 |

where

$$C_P = C_t \left(T_b - 25\right),$$
$$C_R = 1 - 0.025 \left(T_b - 25\right),$$
$$R = \frac{N_{B\text{-}s} V_n \left(1 - \eta\right) C_R}{\left(0.2 N_{B\text{-}p} Q_n\right)}, \tag{6}$$
$$\mathrm{SOC} = \frac{N_{B\text{-}s} N_{B\text{-}p} Q_n - \int_0^t i_B(\tau)\, d\tau}{N_{B\text{-}s} N_{B\text{-}p} Q_n} \times 100\%,$$

where SOC is the state of charge that describes the instantaneous charge of the battery stack or the amount of electric energy stored in the battery stack at any instant in time, $C_p$ is the temperature compensation factor of polarization effect, $C_R$ is temperature compensation factor of resistance, $E_0$ is the initial moment the electric potential of battery cell, and $V$ is the output voltage of lead-acid battery. The total power contribution to the hybrid system from the battery stack can be given as

$$P_B = i_B V_B \left(1 - K_{\text{B-loss}}\right). \tag{7}$$

Proton exchange membrane (PEM) FC is employed in the hybrid system as backup generator [31–33]. When the SOC of the battery bank is lower than 25%, the PEM FC is turned on to supply the load demand; otherwise it will

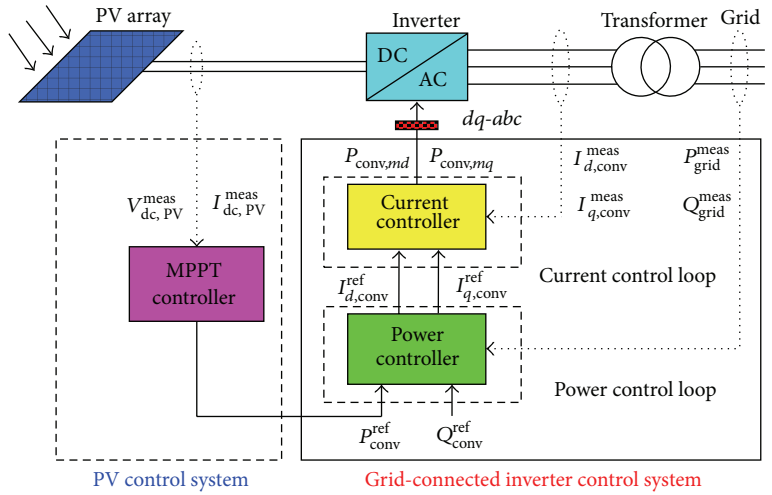


Figure 5: Block diagram of the overall control scheme for the PV unit.

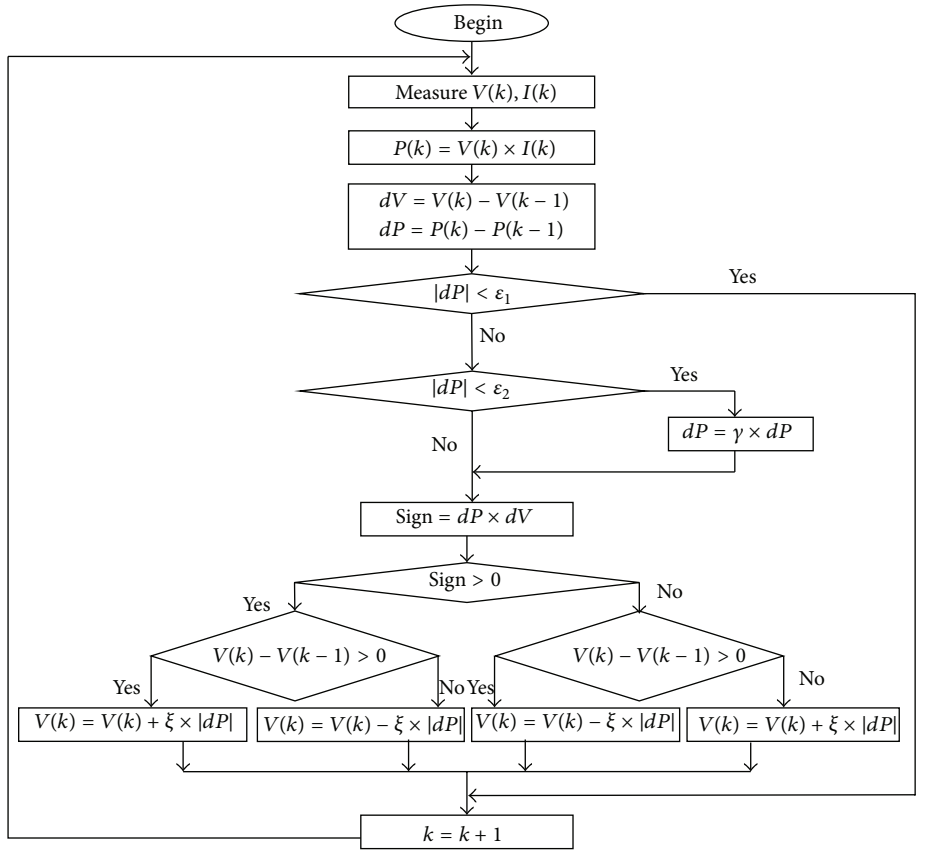


Figure 6: Flowchart of the MPPT algorithm with improved P&O based on power change rate.

be turned off. The modeling of the PEM FC consists of the relationship between electrical energy production and the consumed hydrogen. Detailed description of PEM FC modeling and polarization characteristics can be found in [32, 33]. Assuming that each cell has equivalent output voltage, the current for the complete stack can be found using the following overall equation for the electrical terminal voltage:

$$V_{FC} = N_{cell\text{-}s}\left[E - \ln\left(\frac{I_{FC} + A_{cell} i_n}{A_{cell} i_o}\right) - r\left(\frac{I_{FC}}{A_{cell}}\right) - m\exp\left(n\frac{I_{FC}}{A_{cell}}\right)\right], \quad (8)$$

where $A_{cell}$ is the electrode area of each cell, $r$ is the area-specific resistance (k$\Omega$ cm$^2$), $i_n$ is the internal and crossover

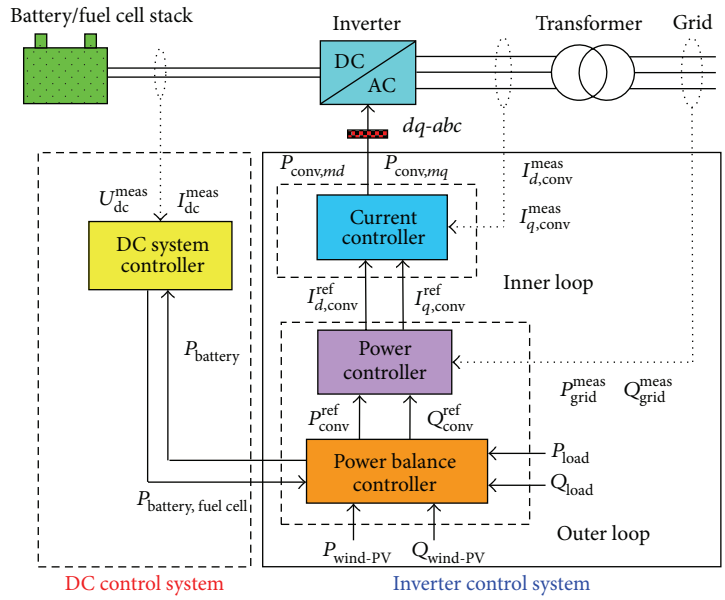


Figure 7: Block diagram of the overall control scheme for the ES unit.

current density (mA/m$^2$), and $m$ and $n$ are constants of the concentration or mass transfer loss parameters. The total power contribution to the hybrid system from the FC unit can be written as

$$P_{FC} = I_{FC} V_{FC} N_{cell\text{-}p}. \quad (9)$$

The details of ES unit dynamic model have been used for all components of the system given in Figure 7. The component parameters of the battery stack and FC unit are presented in Table 3. The rating capacity of the battery or FC energy system, which consists of 200 battery or FC stacks (as shown in Figure 7), is 100 MW.

## 4. Overall Coordinated Control Strategy

An overall coordinated control strategy for power management among different energy sources in a multisources energy system is needed [34, 35]. The block diagram of the control strategy for the proposed hybrid energy generation system is shown in Figure 8. The WECS, controlled by a pitch angle controller, and a PV generation system, controlled by a MPPT controller, are the primary energy sources of the hybrid generation system. When the energy generated from the WECS and PV system becomes insufficient with respect to the load demand, the shortage power is compensated by ES system. The tracking mismatches of the wind-PV system and the load demand exceeding the power generated by the WECS and PV system, is fed to the battery stack. STATCOM is used to adjust reactive power to support bus voltage and improve LVRT capability of the hybrid system.

*4.1. Active Power Coordinated Control Strategy.* The active power difference between the generation sources and the load demand given by the power network dispatching center is calculated as

$$P_{net} = P_{wind} + P_{PV} - P_{load} - P_{sc}, \quad (10)$$

Table 3: ES system component parameters.

| Parameter | Value |
|---|---|
| Battery stack | |
| Rated capacity, $Q_n$ | 200 Ah |
| Rated voltage, $V_n$ | 2 V |
| Efficiency of a battery, $\eta$ | 0.985 |
| Temperature of battery, $T_b$ | 25°C |
| Polarization voltage constant, $K$ | 0.051 |
| Polarization effect coefficient, $C_t$ | 0.011 |
| Voltage change factor, $A$ | 0.005 |
| Capacity change factor, $B$ | 0.6 |
| Dynamic link loss factor, $K_{B\text{-loss}}$ | 0.05 |
| Number of series modules, $N_{B\text{-}s}$ | 350 |
| Number of parallel modules, $N_{B\text{-}p}$ | 22 |
| FC unit | |
| Rating | 1.2 kW |
| Rated current, $I_{FC}$ | 45 A |
| Rated voltage, $V_{FC}$ | 28 V |
| Number of series modules, $N_{cell\text{-}s}$ | 25 |
| Number of parallel modules, $N_{cell\text{-}p}$ | 17 |
| Proportional and integral gain of controller | |
| $K_p$ of power controller | 5 |
| $T_i$ of power controller | 0.15 |
| $K_p$ of current controller | 0.0382 |
| $T_i$ of current controller | 0.013 |

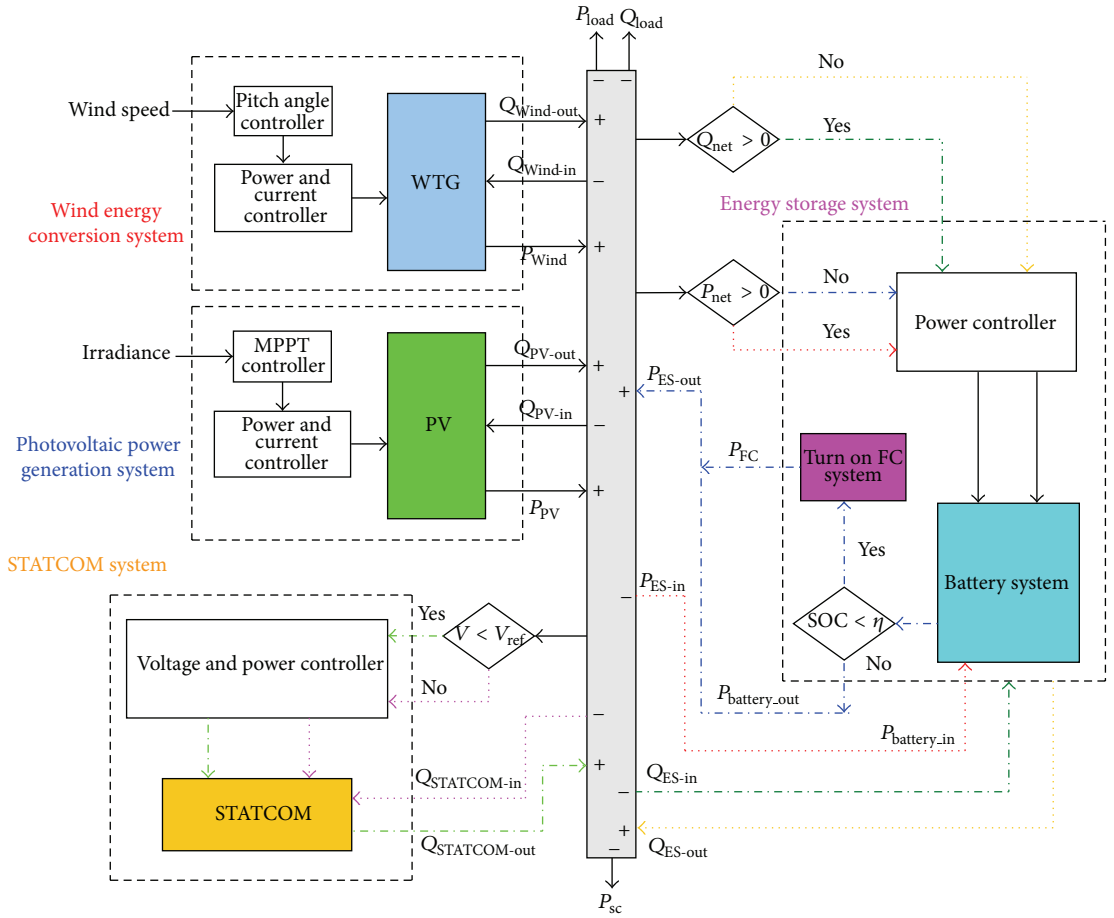


FIGURE 8: Block diagram of overall coordinated control scheme for grid-connected wind/PV/ES and STATCOM hybrid energy conversion system.

where $P_{wind}$ is the active power generated by the WECS, $P_{PV}$ is the active power generated by the PV energy conversion system, $P_{load}$ is the active power demand given by the power network dispatching center, and $P_{sc}$ is the self-consumed active power for operating the system. The system self-consumed active power is the power consumed by the auxiliary system components to keep it running, for example, the active power needed for running the cooling systems, the control units, and the lighting system. For simplification, only the active power consumed by the ES system is considered in this study.

The coordinated control strategy is that, at any given time, any excess wind and PV-generated active power ($P_{net} > 0$) is stored in the battery stack. Therefore, the active power balance equation given in (10) can be written as

$$P_{wind} + P_{PV} = P_{load} + P_{ES\text{-}in}, \qquad P_{net} > 0, \tag{11}$$

where $P_{ES\text{-}in}$ is the power consumed by the battery stack ($P_{battery\_in}$).

When there is a deficit in active power generation ($P_{net} < 0$), the battery stack begins to supply energy for power network. When the SOC of battery is lower than $\eta$, the FC system is started as a backup generator. Therefore, the active power balance equation for this situation can be written as

$$P_{wind} + P_{PV} + P_{ES\text{-}out} = P_{load}, \qquad P_{net} < 0, \tag{12}$$

where

$$P_{ES\text{-}out} = P_{battery\_out} + P_{FC}, \tag{13}$$

where $P_{battery\_out}$ and $P_{FC}$ are the active power generated by the battery stack and FC unit, respectively.

*4.2. Reactive Power Coordinated Control Strategy.* The power factor of the proposed hybrid system is regulated between 0.95 lagging and 0.95 leading. Wind/PV energy conversion system runs in 0.98 (lag), normally [36]. The reactive power difference between the generation sources and the load demand given by the power network dispatching center is calculated as

$$Q_{net} = Q_{Wind\text{-}out} + Q_{PV\text{-}out} - Q_{load}, \tag{14}$$

where $Q_{Wind\text{-}out}$ is the reactive power generated by WECS, $Q_{PV\text{-}out}$ is the reactive power generated by the PV generation system, and $Q_{load}$ is the reactive power demand given by the power network dispatching center.

The reactive power management control strategy is that any excess wind and PV-generated reactive power ($Q_{net} > 0$) is consumed by the ES system (battery stack or FC unit). At the same time, the extra reactive power is absorbed by STATCOM ($V > V_{ref}$). Therefore, the power balance equation given in (14) can be written as

$$Q_{Wind\text{-}out} + Q_{PV\text{-}out} = Q_{load} + Q_{ES\text{-}in} + Q_{STATCOM\text{-}in}, \quad Q_{net} > 0 \quad V > V_{ref}, \tag{15}$$

where $Q_{ES\text{-}in}$ is the reactive power consumed by ES system, $Q_{STATCOM\text{-}in}$ is the reactive power absorbed by STATCOM, and $V$ and $V_{ref}$ are the hybrid system operated and rated voltage, respectively.

When there is a deficit in reactive power generation ($Q_{net} < 0$), the ES system and STATCOM begin to compensate reactive power for the power network. Therefore, the power balance equation for this situation can be written as

$$Q_{load} = Q_{Wind\text{-}out} + Q_{PV\text{-}out} + Q_{ES\text{-}out} + Q_{STATCOM\text{-}out}, \quad Q_{net} < 0 \quad V < V_{ref}, \tag{16}$$

or

$$Q_{load} + Q_{STATCOM\text{-}in} = Q_{Wind\text{-}out} + Q_{PV\text{-}out} + Q_{ES\text{-}out}, \quad Q_{net} < 0 \quad V > V_{ref}, \tag{17}$$

where $Q_{ES\text{-}out}$ is the reactive power supplied by ES system, $Q_{STATCOM\text{-}in}$ is the reactive power generated by STATCOM.

When wind/PV energy conversion system runs in 0.98 (lead) ($Q_{net} < 0$), the ES system compensates reactive power for the system. The reactive power of STATCOM is governed by the bus voltage of grid-connected point. Therefore, the reactive power balance equation can be written as

$$Q_{Wind\text{-}in} + Q_{PV\text{-}in} + Q_{load} = Q_{ES\text{-}out} + Q_{STATCOM\text{-}out}, \quad Q_{net} < 0 \quad V < V_{ref}, \tag{18}$$

or

$$Q_{Wind\text{-}in} + Q_{PV\text{-}in} + Q_{load} + Q_{STATCOM\text{-}in} = Q_{ES\text{-}out}, \quad Q_{net} < 0 \quad V > V_{ref}, \tag{19}$$

where $Q_{Wind\text{-}in}$ and $Q_{PV\text{-}in}$ are the reactive power absorbed by WECS and PV system, respectively.

Large scale grid-connected hybrid generation system should satisfy LVRT requirement when a grid fault occurs, and the system including STATCOM has the advantage of satisfying LVRT. STATCOM has been identified as the fastest responding device that can assist in improving the power quality and stability of the system.

Dynamic models have been used for all the components of the hybrid system shown in Figure 8. The details of these models are given in Figures 2–7, respectively.

## 5. Simulation Results

Using the component models discussed in Section 4, the simulation system based on 3-machine 9-bus test system of Western System Coordinating Council (WSCC) [37] and the proposed large scale wind/PV/ES/STATCOM hybrid system have been developed using DIgSILENT/Power Factory software platform. The wind/PV/ES/STATCOM hybrid generation system discussed in Section 3 was connected on the bus 6 of the WSCC 3-machine 9-bus test system depicted in Figure 9. In order to verify the system performance under different situations, simulation studies have been carried out using practical load demand profiles and real weather data (wind speed, solar irradiance, and air temperature). The typical hourly average load demand and weather data for the China Northeast regions are used in this simulation study. Simulation studies are carried out for power coordinated control during a winter day and a summer day. Simulation results for the winter and summer scenarios are given and discussed in the following section.

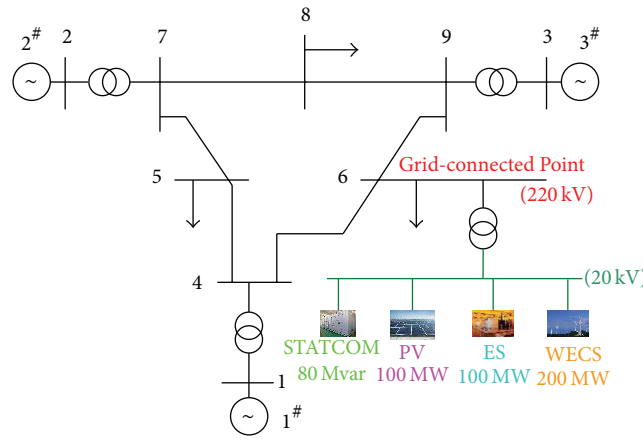


Figure 9: Single line diagram of the studied power system.

### 5.1. Winter Scenario

*5.1.1. Load and Weather Data.* The load demand data for the winter scenario simulation collected on December 17, 2010, is shown in Figure 10. Figure 11 shows the hourly wind speed profile over 24 h on the day (December 17, 2010) the data were collected. The hourly solar irradiance data and air temperature collected on the same day are shown in Figures 12 and 13, respectively.

*5.1.2. Simulation Result.* The system performance under the load profile given in Figure 10 and the weather data shown in Figures 11–13 is evaluated and discussed later.

The output power and pitch angle from the wind energy conversion unit in the hybrid energy generation system over the 24 h simulation period are shown in Figures 14 and 15, respectively. The pitch angle of the blade should be controlled to protect the turbines as well as to limit the output power at high wind speed [38]. Below the rated wind speed (shown in Figure 3), the blade pitch angle is usually set to produce the maximum output power. Above the rated wind speed, the blade pitch angle is regulated for the output power to be limited at the rated value of generators.

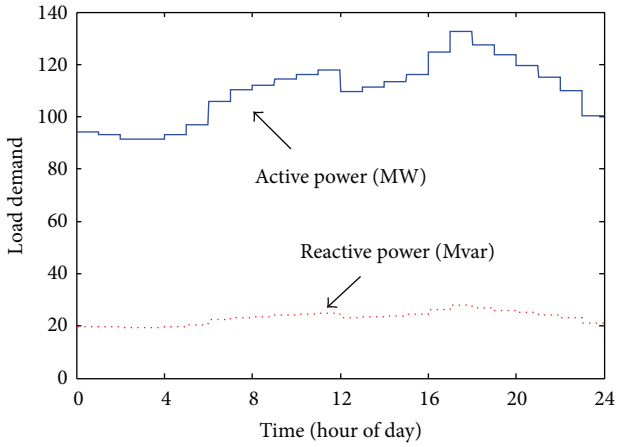


Figure 10: Hourly load profile for the winter scenario simulation study in northeast China.

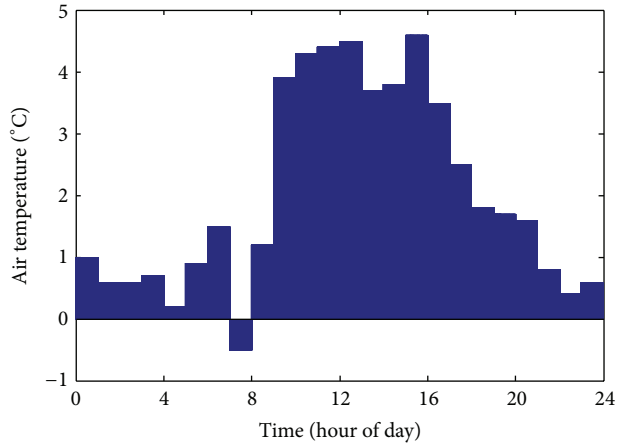


Figure 13: Air temperature data for the winter scenario simulation study in northeast China.

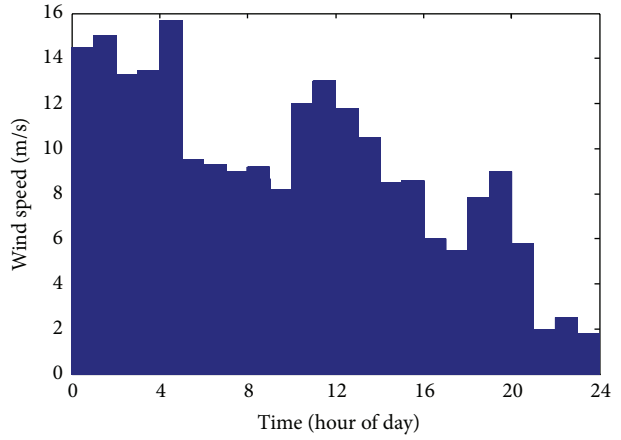


Figure 11: Wind speed data for the winter scenario simulation study in northeast China.

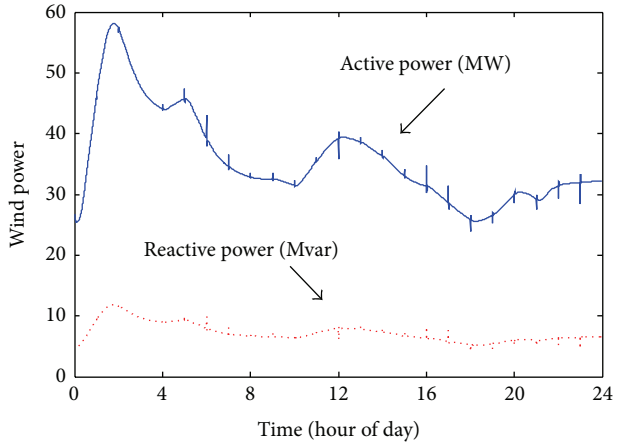


Figure 14: Wind power for the winter scenario simulation study.

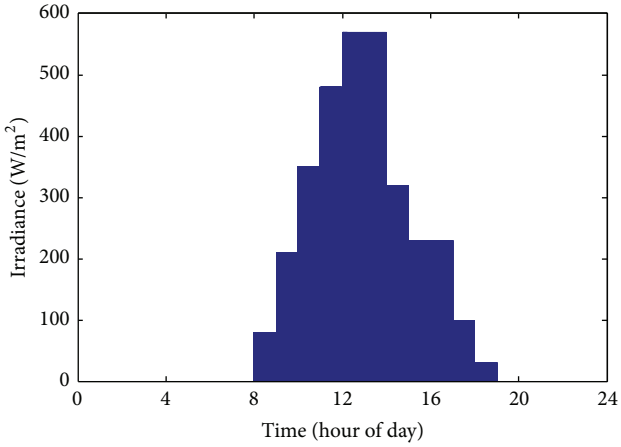


Figure 12: Solar irradiance data for the winter scenario simulation study in northeast China.

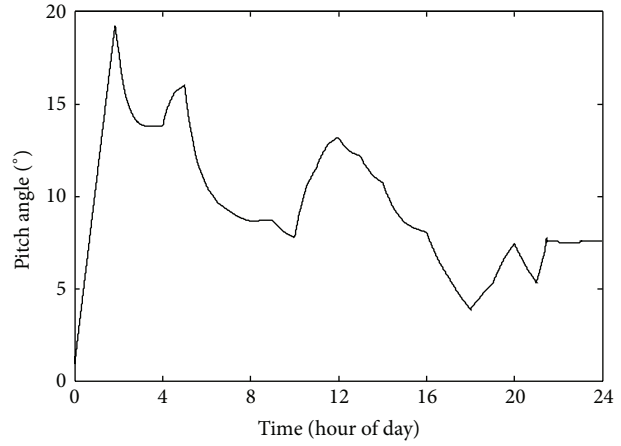


Figure 15: Pitch angle for the winter scenario simulation study.

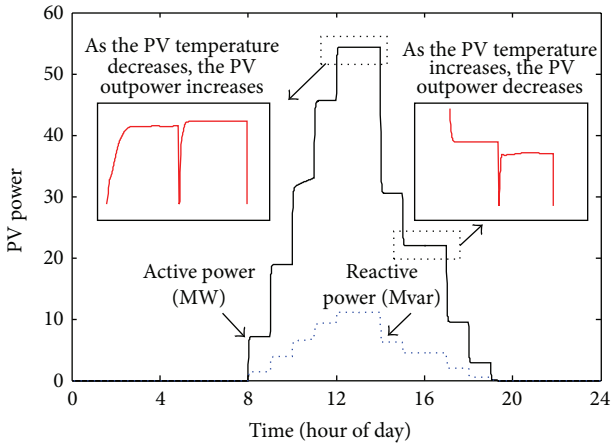


FIGURE 16: PV power for the winter scenario simulation study.

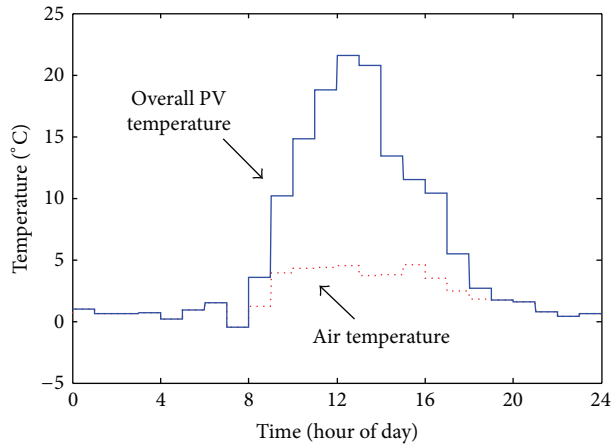


FIGURE 17: PV temperature response over the simulation period for the winter scenario.

The output power from the PV system in the hybrid system over the 24 h simulation period is shown in Figure 16. As shown in Figure 8, the PV array output power is controlled by an MPPT controller (discussed in Section 3.2) to give maximum power output under different solar irradiances. It is noted that the PV output power curve, shown in Figure 16, has a wave shape similar to that of the solar irradiance profile shown in Figure 12.

Temperature plays an important role in PV module's performance. Figure 17 shows the PV temperature response over the simulation period. Two main factors for determining the temperature of the PV module are the solar irradiance (Figure 12) and the surrounding air temperature (Figure 13). Figures 16 and 17 also show the effect of temperature upon the PV performance.

When $P_{net} < 0$ (see (7), (9), and (10)), the sum of wind and PV-generated active power is not sufficient to supply the load demand. Under this condition, the battery stack turns on to supply the active power shortage. If SOC < 25%, the battery stack is replaced by the FC system. Figures 18 and 19 show the actual power delivered by the ES system that included battery stack and FC unit.

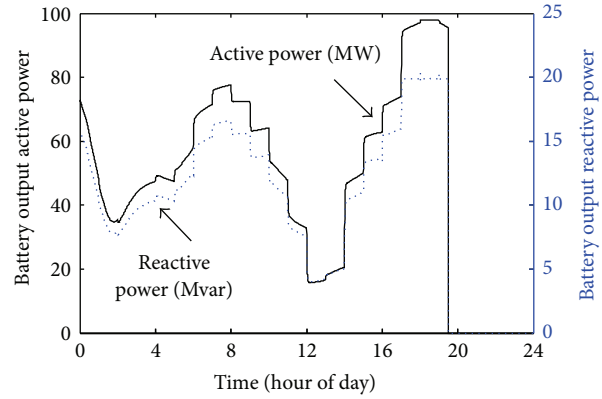


FIGURE 18: Power supplied by battery stack for the winter scenario simulation study.

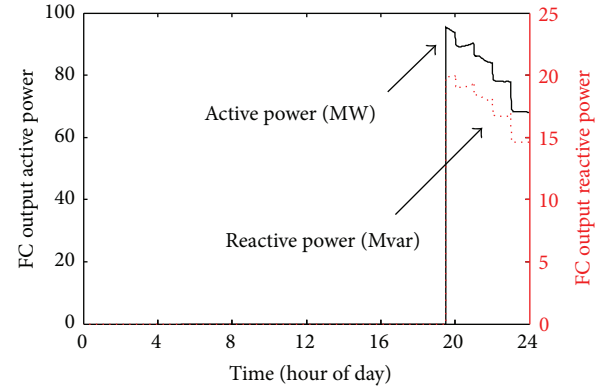


FIGURE 19: Power supplied by FC for the winter scenario simulation study.

When the power factor of wind/PV hybrid generation system runs in 0.98 (lag) and $Q_{net} < 0$ (see (11), (13), and (14)), the sum of wind and PV-generated reactive power is not sufficient to supply the load demand. The ES system supplies reactive power for load demand. When the reactive power compensated by ES system is a deficit, STATCOM deliveries the deficit reactive power and maintains voltage at a higher operating level. Figure 20 shows the reactive power delivered by STATCOM and the bus voltage level of the hybrid generation system.

### 5.2. Summer Scenario

*5.2.1. Load and Weather Data.* The load demand data for the summer scenario simulation collected on July 16, 2010, is shown in Figure 21. The weather data collected in Northeast China, on July 16, 2010, are used for the summer scenario study. The wind speed data is shown in Figure 22. The solar irradiance and air temperature data at the same site on the same day are shown in Figures 23 and 24, respectively.

*5.2.2. Simulation Results.* The system performance under the load profile given in Figure 21 and the weather data shown in Figures 22–24 is evaluated and discussed later. The output

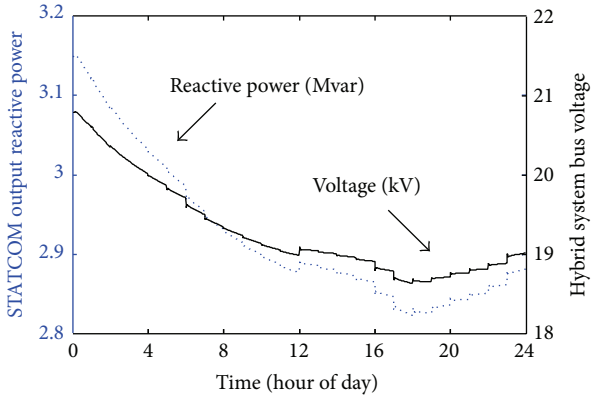


Figure 20: Reactive power supplied by STATCOM and hybrid system bus voltage for the winter scenario simulation study.

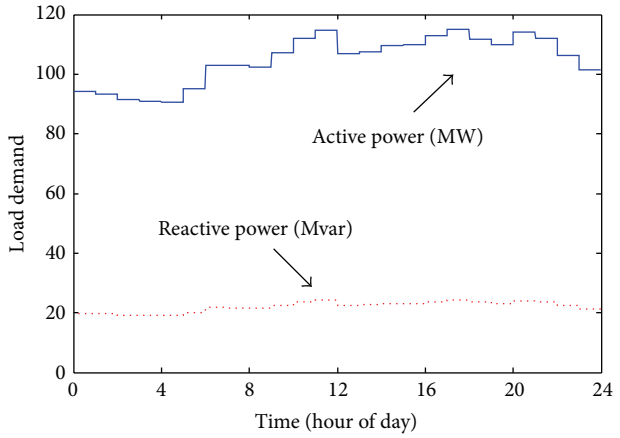


Figure 21: Hourly load profile for the summer scenario simulation study in northeast China.

power from the WECS and the PV energy conversion system in the hybrid generation system over the 24 h simulation period are shown in Figures 25 and 26, respectively. The transient responses of MPPT (discussed in Figure 6) shown in Figure 26 are due to keeping the PV array operating at its maximum power points under different temperatures and solar irradiances.

When $P_{\text{net}} > 0$ (see (7) and (8)), there is excess active power available for battery. Figure 27 shows the available active power profile over the 24 h simulation period. When $P_{\text{net}} > 0$, the sum of the wind and PV-generated active power is not sufficient to supply the load demand. Under this scenario, the battery stack or the FC unit (when SOC < 25%) turns on to supply the active power shortage. Figures 27 and 28 show the actual active power supplied by the battery stack and the FC unit, respectively. The SOC of the battery stack over the simulation period is shown in Figure 29.

In this scenario, WECS under the same power factor with the winter scenario, PV energy system runs in 0.98 (lead). The output reactive power from the WECS and the PV generation system in the hybrid energy system over the 24 h simulation period are given in Figures 25 and 26, respectively.

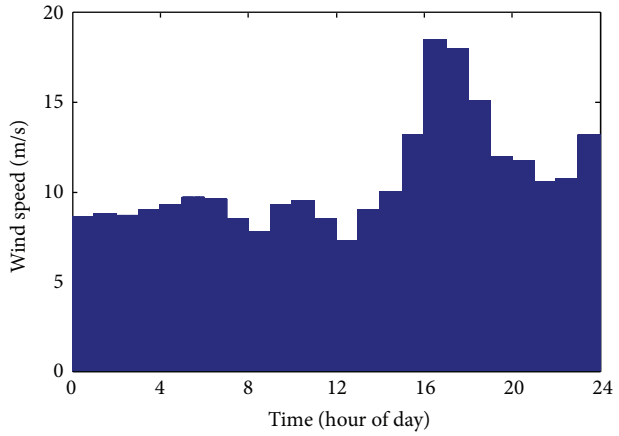


Figure 22: Wind speed for the summer scenario simulation study in northeast China.

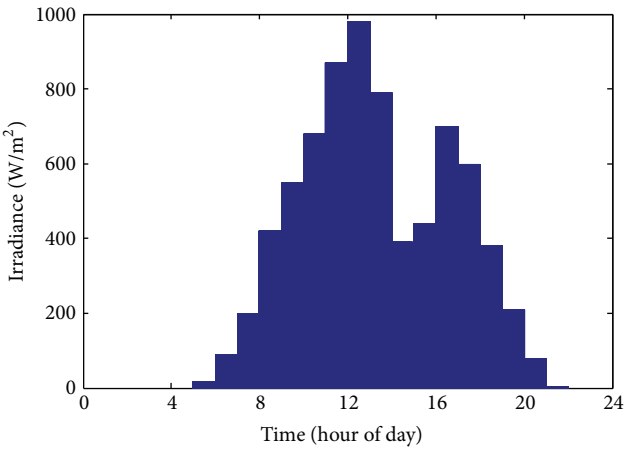


Figure 23: Solar irradiance data for the summer scenario simulation study in Northeast China.

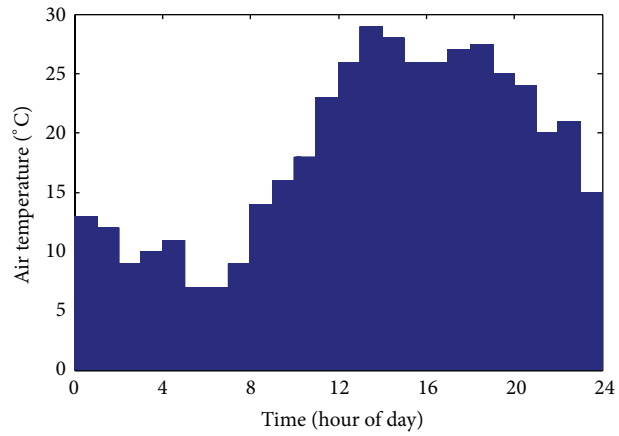


Figure 24: Air temperature data for the summer scenario simulation study in Northeast China.

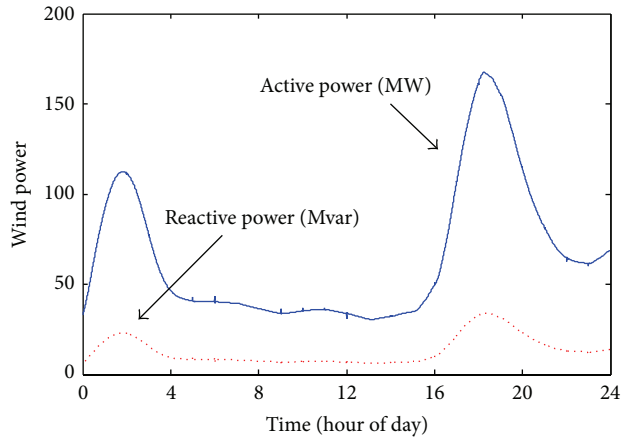


Figure 25: Wind power for the summer scenario simulation study.

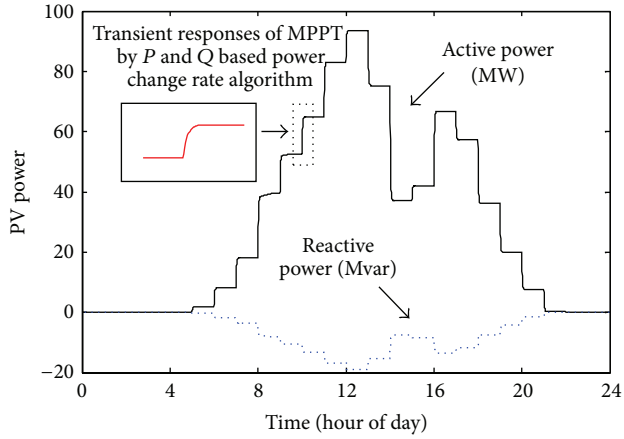


Figure 26: PV power for the summer scenario simulation study.

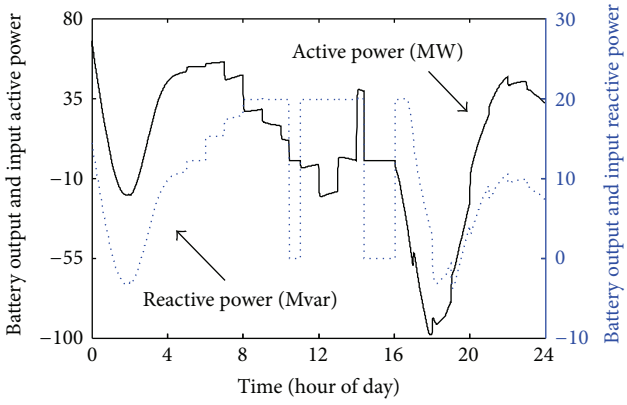


Figure 27: Battery stack power supplied and absorbed for the summer scenario simulation study.

When $Q_{net} > 0$ and $V > V_{ref}$ (see (11) and (12)) the excess reactive power is consumed by the battery stack. If the excess reactive power mismatches with the reactive limit consumed by battery stack, STATCOM states to regulate the excess reactive power together with the battery stack. When $Q_{net} < 0$ (see (12) and (14)–(17)) the deficit of reactive

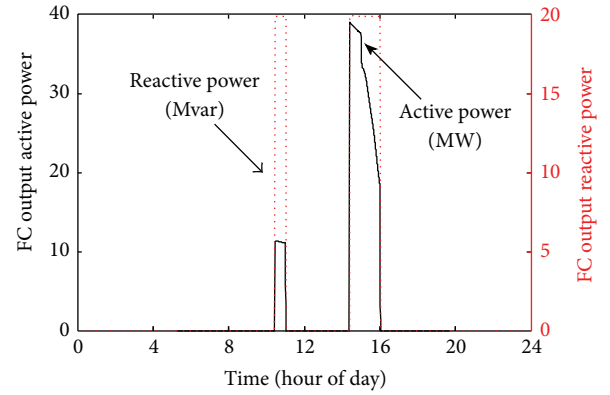


Figure 28: FC power generated for the summer scenario simulation study.

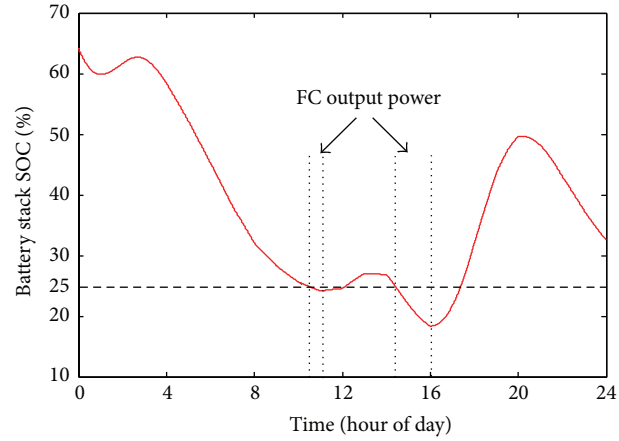


Figure 29: Battery stack SOC over 24 h for the summer scenario simulation study.

power is compensated by the battery stack and FC unit. If the reactive power generated battery stack and FC unit cannot satisfy reactive power demand, STATCOM is stated for the deficit of reactive power. Figures 27, 28, and 30 show the consumed or compensated reactive power profile over the 24 h simulation period. Bus voltage levels of the system over the 24 h simulation period for different combination mode are shown in Figure 31.

In order to analyze the extent to which the LVRT capability of the Wind/PV/ES energy generation system can be enhanced by using STATCOM, a three-phase short circuit to ground fault has been simulated. From Figure 32, it is clear that the STATCOM can improve the LVRT capability and bus voltage level of the hybrid energy conversion system, obviously.

## 6. Conclusion

In this paper, a grid-connected wind/PV/FC hybrid energy generation system is proposed. The system configuration is discussed; the characteristics of the primary components in the system, namely, the WECS, PV, battery, and FC, are given; and the overall coordinated control strategy for the

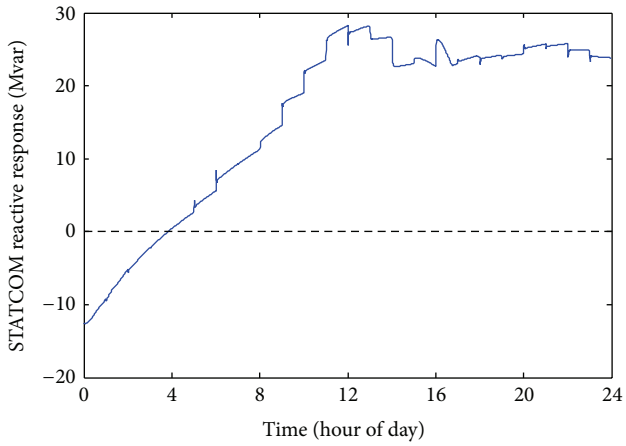


Figure 30: STATCOM reactive power supplied and absorbed for the summer scenario simulation study.

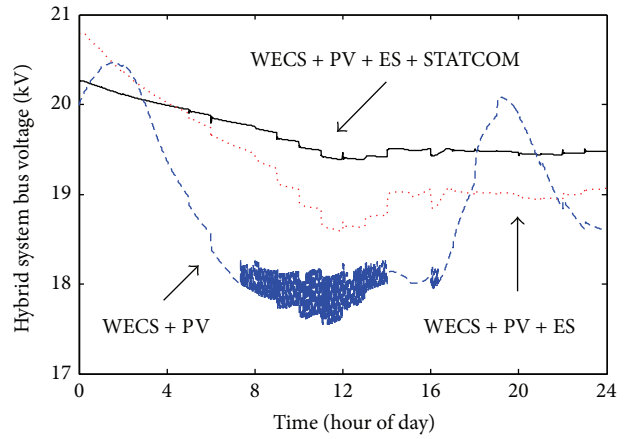


Figure 31: Hybrid system bus voltage under different operating conditions for the summer scenario simulation study.

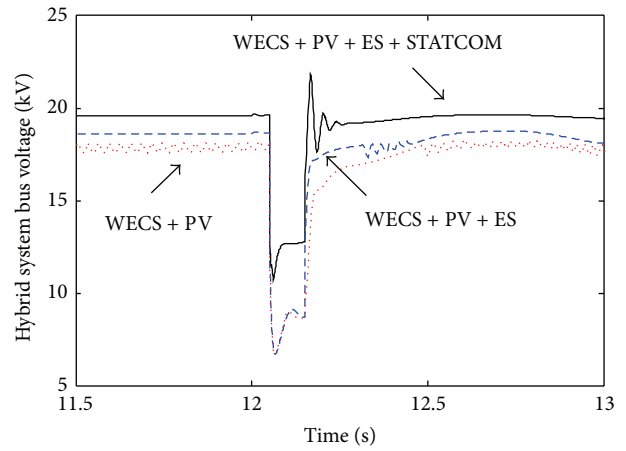


Figure 32: Hybrid system transient voltage during the short circuit fault for different operating conditions.

proposed hybrid energy system is presented. The wind and PV generation systems are the main power generation devices, and the battery stack acts as a dump load to store any excess power available. The FC unit is the backup generation and supplies power to the system when SOC < 25%. The simulation model of the hybrid system has been developed using the DIgSILENT/Power Factory. Simulation studies have been carried out to verify the system performance under different scenarios using the practical load profile in the China northeast regions and the real weather data collected at Shenyang, China. The simulation results, given for a winter and a summer scenario, show the effectiveness of the overall coordinated control strategy and the feasibility of the proposed grid-connected hybrid energy conversion system.

## Conflict of Interests

The authors declare that there is no conflict of interests regarding the publication of this paper.

## Acknowledgments

The authors gratefully acknowledge the support of the National High Technology Research and Development Program (863 Program) of China (no. SS2014AA052502), Changjiang Scholars and Innovative Research Team in University (No. IRT1114), the National Natural Science Foundation of China (nos. 51177010 and 51377017), and the Foundation of the Jilin Technology Development Program (nos. 20140203003SF and 20150411008XH).

## References

[1] C. Rubbia, "Today the world of tomorrow-the energy challenge," *Energy Conversion and Management*, vol. 47, no. 17, pp. 2695–2697, 2006.

[2] D. P. Papadopoulos and J. C. Dermentzoglou, "Economic viability analysis of planned WEC system installations for electrical power production," *Renewable Energy*, vol. 25, no. 2, pp. 199–217, 2002.

[3] Z. Chen, J. M. Guerrero, and F. Blaabjerg, "A review of the state of the art of power electronics for wind turbines," *IEEE Transactions on Power Electronics*, vol. 24, no. 8, pp. 1859–1875, 2009.

[4] S. B. Skretas and D. P. Papadopoulos, "Efficient design and simulation of an expandable hybrid (wind-photovoltaic) power system with MPPT and inverter input voltage regulation features in compliance with electric grid requirements," *Electric Power Systems Research*, vol. 79, no. 9, pp. 1271–1285, 2009.

[5] O. Ozgener, "A small wind turbine system (SWTS) application and its performance analysis," *Energy Conversion and Management*, vol. 47, no. 11-12, pp. 1326–1337, 2006.

[6] P. Wang and R. Billinton, "Reliability benefit analysis of adding WTG to a distribution system," *IEEE Transactions on Energy Conversion*, vol. 16, no. 2, pp. 134–139, 2001.

[7] K. Agbossou, M. Kolhe, J. Hamelin, and T. K. Bose, "Performance of a stand-alone renewable energy system based on energy storage as hydrogen," *IEEE Transactions on Energy Conversion*, vol. 19, no. 3, pp. 633–640, 2004.

[8] H. Zhang, J. Wang, and Y. Shi, "Robust $H_\infty$ sliding-mode control for Markovian jump systems subject to intermittent observations and partially known transition probabilities," *Systems and Control Letters*, vol. 62, no. 12, pp. 1114–1124, 2013.

[9] D. B. Nelson, M. H. Nehrir, and C. Wang, "Unit sizing and cost analysis of stand-alone hybrid wind/PV/fuel cell power generation systems," *Renewable Energy*, vol. 31, no. 10, pp. 1641–1656, 2006.

[10] L. B. Wu, Z. M. Zhao, and J. Z. Liu, "A single-stage three-phase grid-connected photovoltaic system with modified MPPT method and reactive power compensation," *IEEE Transactions on Energy Conversion*, vol. 22, no. 4, pp. 881–886, 2007.

[11] Y.-H. Kim and S.-S. Kim, "An electrical modeling and fuzzy logic control of a fuel cell generation system," *IEEE Transactions on Energy Conversion*, vol. 14, no. 2, pp. 239–244, 1999.

[12] T. Zhou, B. Francois, M. el Hadi Lebbal, and S. Lecoeuche, "Real-time emulation of a hydrogen-production process for assessment of an active wind-energy conversion system," *IEEE Transactions on Industrial Electronics*, vol. 56, no. 3, pp. 737–746, 2009.

[13] A. A. Solomon, D. Faiman, and G. Meron, "Properties and uses of storage for enhancing the grid penetration of very large photovoltaic systems," *Energy Policy*, vol. 38, no. 9, pp. 5208–5222, 2010.

[14] C. S. Wang and M. H. Nehrir, "Power management of a stand-alone wind/photovoltaic/fuel cell energy system," *IEEE Transactions on Energy Conversion*, vol. 23, no. 3, pp. 957–967, 2008.

[15] H. Zhang, Y. Shi, and J. Wang, "On energy-to-peak filtering for nonuniformly sampled nonlinear systems: a markovian jump system approach," *IEEE Transactions on Fuzzy Systems*, vol. 22, no. 1, pp. 212–222, 2014.

[16] N. A. Ahmed and M. Miyatake, "A stand-alone hybrid generation system combining solar photovoltaic and wind turbine with simple maximum power point tracking control," in *Proceedings of the CES/IEEE 5th International Power Electronics and Motion Control Conference (IPEMC '06)*, vol. 1, pp. 1–7, Shanghai, China, August 2006.

[17] J. B. Ekanayake, L. Holdsworth, X. G. Wu, and N. Jenkins, "Dynamic modeling of doubly fed induction generator wind turbines," *IEEE Transactions on Power Systems*, vol. 18, no. 2, pp. 803–809, 2003.

[18] I. Erlich, J. Kretschmann, J. Fortmann, S. Mueller-Engelhardt, and H. Wrede, "Modeling of wind turbines based on doubly-fed induction generators for power system stability studies," *IEEE Transactions on Power Systems*, vol. 22, no. 3, pp. 909–919, 2007.

[19] G. Cai, L. Kong, and D. Yang, "Research on modelling and operation characteristics analysis of large-scale wind & light complementary electricity-generating system," *Power System Technology*, vol. 36, no. 1, pp. 65–71, 2012.

[20] H. Zhang, X. Zhang, and J. Wang, "Robust gain-scheduling energy-to-peak control of vehicle lateral dynamics stabilisation," *Vehicle System Dynamics*, vol. 52, no. 3, pp. 309–340, 2014.

[21] S. K. Kim, J. H. Jeon, C. H. Cho, E. S. Kim, and J. B. Ahn, "Modeling and simulation of a grid-connected PV generation system for electromagnetic transient analysis," *Solar Energy*, vol. 83, no. 5, pp. 664–678, 2009.

[22] B. Yang, W. Li, Y. Zhao, and X. He, "Design and analysis of a grid-connected photovoltaic power system," *IEEE Transactions on Power Electronics*, vol. 25, no. 4, pp. 992–1000, 2010.

[23] A. Yazdani and P. P. Dash, "A control methodology and characterization of dynamics for a photovoltaic (PV) system interfaced with a distribution network," *IEEE Transactions on Power Delivery*, vol. 24, no. 3, pp. 1538–1551, 2009.

[24] M. A. S. Masoum, H. Dehbonei, and E. F. Fuchs, "Theoretical and experimental analyses of photovoltaic systems with voltage- and current-based maximum power-point tracking," *IEEE Transactions on Energy Conversion*, vol. 17, no. 4, pp. 514–522, 2002.

[25] Y. T. Tan, D. S. Kirschen, and N. Jenkins, "A model of PV generation suitable for stability analysis," *IEEE Transactions on Energy Conversion*, vol. 19, no. 4, pp. 748–755, 2004.

[26] H. Zhang, Y. Shi, and B. Mu, "Optimal $H_\infty$-based linear-quadratic regulator tracking control for discrete-time takagi-sugeno fuzzy systems with preview actions," *Journal of Dynamic Systems, Measurement and Control*, vol. 135, no. 4, Article ID 044501, 2013.

[27] S. Tian, M. Hong, and M. G. Ouyang, "An experimental study and nonlinear modeling of discharge I-V behavior of valve-regulated lead-acid batteries," *IEEE Transactions on Energy Conversion*, vol. 24, no. 2, pp. 452–458, 2009.

[28] J. Zhang, S. Ci, H. Sharif, and M. Alahmad, "Modeling discharge behavior of multicell battery," *IEEE Transactions on Energy Conversion*, vol. 25, no. 4, pp. 1133–1141, 2010.

[29] N. A. Ahmed, A. K. Al-Othman, and M. R. Alrashidi, "Development of an efficient utility interactive combined wind/photovoltaic/fuel cell power system with MPPT and DC bus voltage regulation," *Electric Power Systems Research*, vol. 81, no. 5, pp. 1096–1106, 2011.

[30] C. Wang, M. H. Nehrir, and S. R. Shaw, "Dynamic models and model validation for PEM fuel cells using electrical circuits," *IEEE Transactions on Energy Conversion*, vol. 20, no. 2, pp. 442–451, 2005.

[31] K. P. Adzakpa, K. Agbossou, Y. Dubé, M. Dostie, M. Fournier, and A. Poulin, "PEM fuel cells modeling and analysis through current and voltage transient behaviors," *IEEE Transactions on Energy Conversion*, vol. 23, no. 2, pp. 581–591, 2008.

[32] N. A. Ahmed, "Computational modeling and polarization characteristics of proton exchange membrane fuel cell with evaluation of its interface systems," *European Power Electronics and Drives Journal*, vol. 18, no. 1, pp. 32–41, 2008.

[33] L. Kong, G. Cai, D. Yang, and Z. Sun, "Modeling and coordinated control of grid-connected PV generation system with energy storage devices," *Power System Technology*, vol. 37, no. 2, pp. 312–318, 2013.

[34] T. F. El-Shatter, M. N. Eskander, and M. T. El-Hagry, "Energy flow and management of a hybrid wind/PV/fuel cell generation system," *Energy Conversion and Management*, vol. 47, no. 9-10, pp. 1264–1280, 2006.

[35] H. Zhang and J. Wang, "Combined feedback-feedforward tracking control for networked control systems with probabilistic delays," *Journal of the Franklin Institute*, vol. 351, no. 6, pp. 3477–3489, 2014.

[36] M. Liserre, R. Teodorescu, and F. Blaabjerg, "Stability of photovoltaic and wind turbine grid-connected inverters for a large set of grid impedance values," *IEEE Transactions on Power Electronics*, vol. 21, no. 1, pp. 263–271, 2006.

[37] P. W. Sauer and M. A. Pai, *Power System Dynamics and Stability*, Prentice Hall, 1998.

[38] W. L. Chen and Y. Y. Hsu, "Unified voltage and pitch angle controller for wind-driven induction generator system," *IEEE Transactions on Aerospace and Electronic Systems*, vol. 44, no. 3, pp. 913–926, 2008.